ARTICLE

OBC
www.rsc.org/obc

Nucleophilic identity substitution reactions. The reaction between ammonia and protonated amines† ‡

Jon K. Laerdahl, Lihn Bache-Andreassen and Einar Uggerud *
Department of Chemistry, University of Oslo, PO Box 1033, Blindern, N-0315 Oslo, Norway. E-mail: einar.uggerud@kjemi.uio.no

Received 28th February 2003, Accepted 30th June 2003
First published as an Advance Article on the web 15th July 2003

The gas phase reactions between NH_3 and the protonated amines $MeNH_3^+$, $EtNH_3^+$, $Pr^iNH_3^+$, and $Bu^tNH_3^+$ have been studied by high level *ab initio* methods. Mass spectrometric experiments yielded no significant reaction products; this result being consistent with the calculated reaction barriers. The potential energy profiles for both nucleophilic substitution (S_N2) and elimination (E2) pathways have been investigated. Both back side Walden inversion (S_NB) and front side (S_NF) nucleophilic reaction profiles have been generated. The S_NB reaction barriers are found to be higher for the more alkyl substituted reaction centres. Reaction barrier trends have been analysed and compared with the results of a similar study of the H_2O–ROH_2^+ system (R = Me, Et, Pr^i, and Bu^t).

Introduction

Every organic chemist would expect the bimolecular nucleophilic substitution (S_N2) reactions,[1,2]

$$Cl^- + R\text{–}Cl \longrightarrow Cl\text{–}R + Cl^-, \qquad (1)$$

with R = Me, Et, Pr^i, and Bu^t to occur *via* back side attack of the nucleophile (Walden inversion) and with corresponding inversion of configuration. She or he would also have learnt that so-called "steric hindrance" would lead to reduced reaction rates and increased reaction barrier heights along the series R = Me, Et, Pr^i, and Bu^t. This prediction is consistent with experimental and theoretical findings for reaction (1) and related systems both in the gas phase and in solution.[2–6]

It is therefore somewhat surprising that for the gas phase S_N2 reactions,

$$H_2O + R\text{–}OH_2^+ \longrightarrow {}^+H_2O\text{–}R + H_2O, \qquad (2)$$

with R = Me, Et, Pr^i, and Bu^t the pathway of front side nucleophilic attack of the water nucleophile (S_NF) and corresponding retention of configuration have been found to be competing with the familiar back side attack and Walden inversion pathway (S_NB) for R = Bu^t and most likely also for R = Pr^i.[7,8] These two pathways are illustrated in Fig. 1, which also contains tentative potential energy profiles or surfaces (PESs) for the two reactions. The double-well reaction profile is characteristic of these gas phase ion–dipole reactions.[9] The ion–dipole complexation energy, the central barrier relative to the reactants and to the ion–dipole complexes are given in the figure as ΔH_{cmpl}, $\Delta H^{\ddagger}$, and $\Delta H^{\ddagger}_{CB}$, respectively. It has also been established, based on both theoretical and experimental investigations,[6–8] that the barrier heights for reactions (2) *decrease* along the series R = Et > Me > Pr^i > Bu^t with the inverse order for reaction rates.[7] For these reactions, it is thus what organic chemists have learnt are the most "sterically hindered" systems that react the fastest, indeed close to the encounter rate of the molecular ions and dipoles in the gas phase for the H_2O–$Bu^tOH_2^+$ system.

Gas phase studies of simple organic reactions, for example nucleophilic substitution reactions,[10–12] have since the 1970's provided a wealth of new insight into organic reactivity. It turns out that many of the established explanations for trends in reactivity that are based on intrinsic molecular properties such as "steric hindrance" in fact are strongly coupled with solvent effects. Experimental and more recently also high quality theoretical gas phase studies thus provide very important tests of previously accepted theories in an environment that is without the complicating interactions of a solvent.

Of particular interest are the *identity* nucleophilic substitution reactions,

$$X^{-/0} + R\text{–}X^{0/+} \longrightarrow X\text{–}R^{0/+} + X^{-/0} \qquad (3)$$

since the barriers of exo- or endothermic non-identity reactions,

$$Y^{-/0} + R\text{–}X^{0/+} \longrightarrow Y\text{–}R^{0/+} + X^{-/0} \qquad (4)$$

may be determined from Marcus theory,[12–16]

$$\Delta H^{\ddagger}_{CB} = \Delta H^{\ddagger}_{CB,0} + \frac{1}{2}\Delta H_{cent} + \frac{(\Delta H_{cent})^2}{16\Delta H^{\ddagger}_{CB,0}} \qquad (5)$$

with the intrinsic barrier given by the additivity postulate,

$$\Delta H^{\ddagger}_{CB,0}(X,Y) = \frac{1}{2}\left(\Delta H^{\ddagger}_{CB}(X,X) + \Delta H^{\ddagger}_{CB}(Y,Y)\right). \qquad (6)$$

This relationship is applicable for the elementary step over the central reaction barrier as illustrated in Fig. 1, where ΔH_{cent} is the exothermicity of this elementary step. Due to these relationships, the identity reactions (3) are fundamentally important, but unfortunately only a very limited number of these reactions have rates that make them favorable for experimental investigations—employing isotope labeled reactants—in the gas phase. This is because very fast reactions have reaction rates close to the encounter rate and the reaction data do not contain information that may be interpreted in terms of a PES with a central barrier. On the other hand, reaction barriers that are of the order of only 15–20 kJ mol^{-1} above the energy of the reactants yield reaction rates that are undetectably slow in mass spectrometric experiments. It should be noted that the reaction system (2) is one of the very few known where useful

† Part II. For Part I, see preceding paper (DOI: 10.1039/b302268d).
‡ Electronic supplementary information (ESI) available: Cartesian coordinates for all species together with imaginary frequencies for the transition structures. See http://www.rsc.org/suppdata/ob/b3/b302270f/

DOI: 10.1039/b302270f

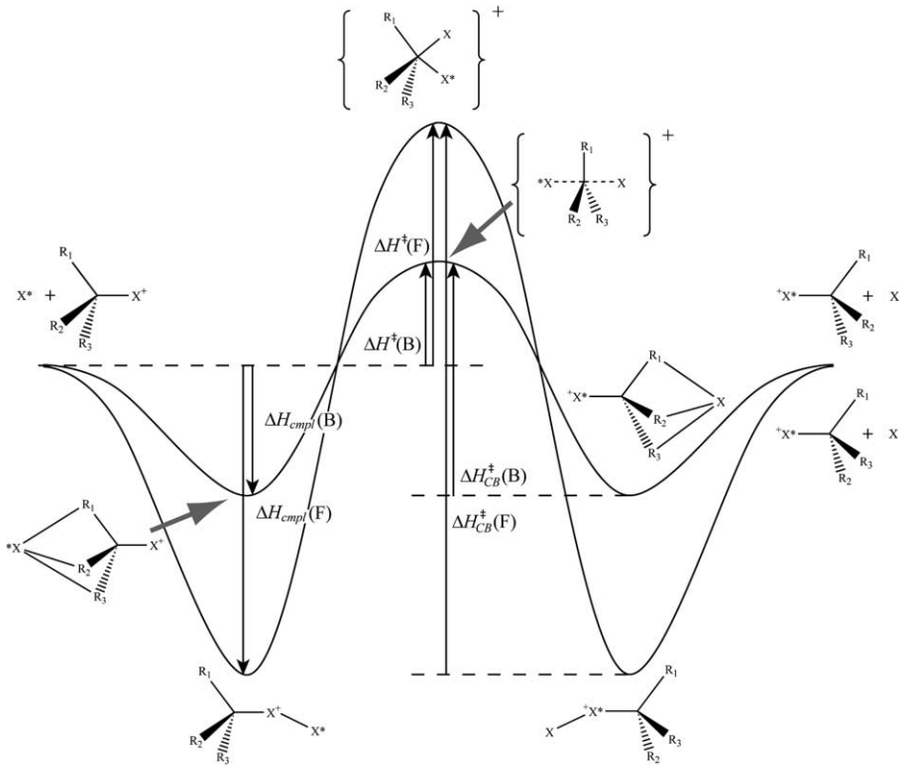

Fig. 1 Potential energy diagram for the Walden inversion back side (B) and the retentitive front side (F) nucleophilic substitution reactions. The identity reaction complexation energy (ΔH_{cmpl}) and the energy barrier relative to the reactants ($\Delta H^{\ddagger}$) and to the ion–dipole complexes ($\Delta H^{\ddagger}_{CB}$) are given in the figure. The indicated relative energies of both complexes (F lower than B) and transition states (B lower than F) are in agreement with the findings for X = H_2O and NH_3 and with R_1, R_2, R_3 = H, CH_3.

PES data may be obtained from experiments on such a broad series of related molecular species.[7] Theoretical *ab initio* calculations do not suffer from the limitations described above, making them extremely useful for accurate studies of small organic reaction systems (less than 6–10 first/second row atoms involved).

The reactions (2) were studied by using high level *ab initio* methods in the first article of this series.[8] In the present article, we discuss work employing the same theoretical methods on the reaction system,

$$NH_3 + R\text{–}NH_3^+ \longrightarrow {}^+H_3N\text{–}R + NH_3, \qquad (7)$$

with R = Me, Et, Pr^i, and Bu^t. Ammonia (proton affinity = 854 kJ mol^{-1}) [17,18] is a slightly stronger nucleophile than water (PA = 691 kJ mol^{-1}),[17,18] but still much weaker than the chlorine anion of reaction (1) (PA = 1395 kJ mol^{-1}).[19] The NH_3–RNH_3^+ reaction system thus bridges the gap between the Cl^-–RCl and H_2O–ROH_2^+ systems which have the normal and inverse dependency on alleged "sterical hindrance", respectively. In related work we have also studied the reactions,

$$HF + R\text{–}FH^+ \longrightarrow {}^+HF\text{–}R + HF, \qquad (8)$$

involving the much weaker nucleophile HF (PA = 484 kJ mol^{-1}),[17,18] and the results will be presented elsewhere.[20] Both S_N2 and the competing elimination (E2) reactions have been investigated for the NH_3–RNH_3^+ system in the present work. The reactions (7) were also studied experimentally employing isotope labeled $^{15}NH_3$ with an instrumental setup similar to the one used for the study of the reactions (2).[7] No significant reaction was detected for any of the reaction systems, R = Me, Et, Pr^i, and Bu^t. This is consistent with the calculated reaction barrier heights. For this reason the experiments will not be described in detail, but further information may be obtained from the authors upon request.

Experimental

Computational details

Ab initio second order Møller–Plesset MP2/6-31G(d) as well as composite method $G2_m$ and $G3_m$ theory have been performed with the Gaussian 98 program.[21] The $G2_m$ and $G3_m$ methods are identical to the standard G2[22] and G3[23] methods, except that zero point vibrational energies (ZPVEs) are calculated at the MP2/6-31G(d) instead of the Hartree–Fock HF/6-31G(d) level. The ZPVEs have been scaled according to Scott and Radom[24] (scaling factor = 0.9434). The final geometry optimizations have also been performed at the MP2/6-31G(d) instead of the MP2(full)/6-31G(d) level. Leaving out the core orbitals in the correlation treatment for the geometry will give negligible errors in the calculations. This has also been demonstrated in the previous article in this series.[8] A number of higher level correlated single-point energy calculations give final $G2_m$ and $G3_m$ energies which are effectively at the QCISD(T)/6-311+G(3df,2p) and QCISD(T)/G3Large level for $G2_m$ and $G3_m$, respectively. For the current closed shell systems we have argued[8,10] that the calculated Gn_m energy barriers and complexation energies are accurate to within less than 10 kJ mol^{-1}.

No symmetry constraints were used in the geometry optimizations. All searches for transition structures were performed with the full analytical Hessian calculated at every step of the geometry optimization. This was necessary due to the very complicated structure of the PES, particularly for the larger molecular species. All energy minima and saddle points were characterized by a full analytic frequency calculation, and intrinsic reaction coordinate (IRC) calculations were performed for all transition structures in order to confirm that they were connecting the expected energy minima. All reported energies are 0 K values including ZPVEs. The MP2/6-31G(d) ZPVEs include a scaling factor[24] = 0.967. The different scaling factor employed in Gn_m theory is due to the 'higher level correction' which we used unchanged from the standard Gn methods.[24]

Vertical electron affinities and ionization potentials were calculated at the CCSD(T)/6-311++G(d,p) level applying the MP2/6-31G(d) geometries and using an unrestricted HF reference for the open shell species. Natural population analysis was performed at the MP2/6-311++G(d,p)//MP2/6-31G(d) level according to Reed *et al.*[25]

Results and discussion

Optimized geometries for the stationary points on the MP2/6-31G(d) PESs for reactions (7) and the competing E2 reactions are given in Figs. 2–5. Cartesian co-ordinates for all species and imaginary frequencies for the transition structures are given in the Supplementary material.‡ Potential energy profiles at the $G3_m$ level for the S_NB, S_NF and E2 pathways have been outlined in Figs. 6–9. Relative energies at the $G3_m$ and MP2/6-31G(d) level have been included in the figures, while $G2_m$ energies only have been calculated for the NH_3–RNH_3^+ (R = Me, Et) systems in Figs. 6–7. The vertical scale is the same in Figs. 6–9.

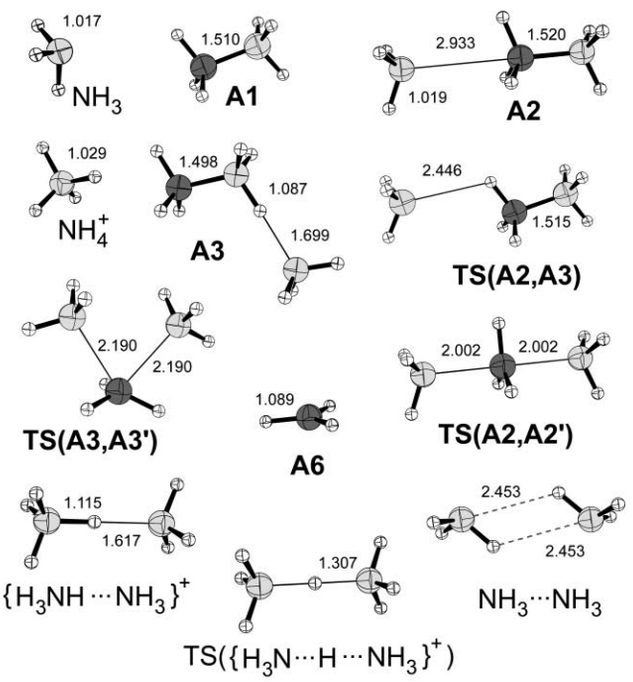

Fig. 2 Structures of stationary points on the PES for the substitution reaction between NH_3 and $MeNH_3^+$ as well as NH_3, NH_4^+, their adduct, and the transition structure for proton transfer between two NH_3 moieties calculated at the MP2/6-31G(d) level. All bond lengths are given in Å. Cartesian coordinates for these structures have been included as Supplementary material.‡

We have earlier shown that the Walden inversion (7) with R = Me is well suited for the Gn_m treatment where the geometries are optimized at the MP2/6-31G(d) level while energy differences are calculated at a higher level of theory (see Table 1 of the first article in this series[8]). We have also argued that non-dynamical correlation is of little importance for the systems studied here as well as for the analogous water–protonated alcohol systems.[8] In conclusion Gn_m methods are expected to give energy barriers and differences of accuracy well below 10 kJ mol^{-1} for the NH_3–RNH_3^+ (R = Me, Et, Pr^i, and Bu^t) systems. Due to the nearly perfect agreement between the $G2_m$ and $G3_m$ results for H_2O–ROH_2^+ (all R)[8] and NH_3–RNH_3^+ (R = Me and Et, see Figs. 6–7) species the costly $G2_m$ calculations were not performed for R = Pr^i and Bu^t. As for H_2O–ROH_2^+ (all R)[8] the complexation energies are overestimated at the MP2/6-31G(d) level relative to the $G3_m/G2_m$ results. The differences are very similar, being approximately 20 and 10 kJ mol^{-1} for the front and rear side complexes, respectively. The MP2/6-31G(d) barrier $\Delta H^{\ddagger}$ also deviates significantly from the

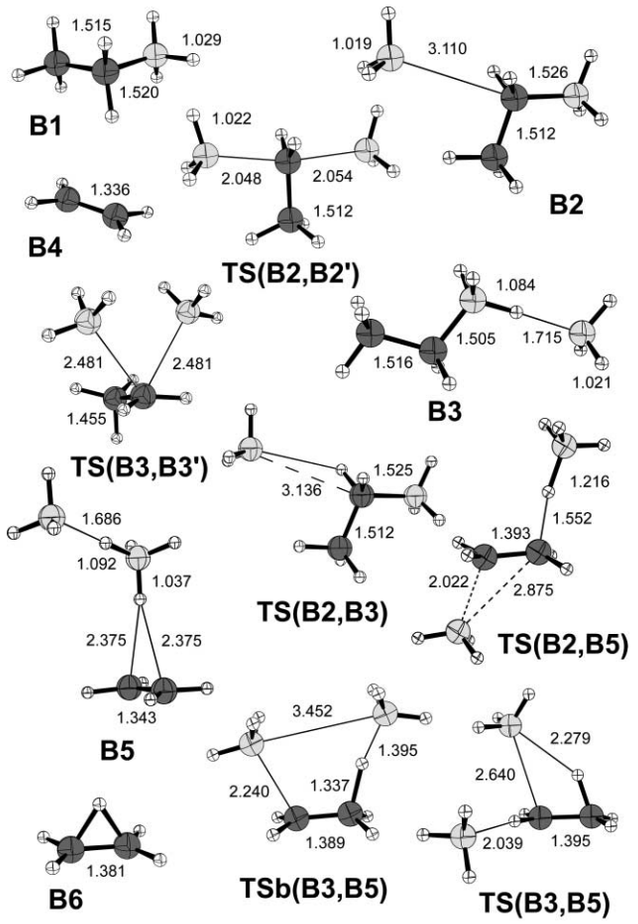

Fig. 3 Structures of stationary points on the PES for the substitution and elimination reaction between NH_3 and $EtNH_3^+$ calculated at the MP2/6-31G(d) level. All bond lengths are given in Å. Cartesian coordinates for these structures have been included as Supplementary material.‡

$G3_m/G2_m$ results, by as much as −13 kJ mol^{-1} for **TS(A2,A2′)** and 12 kJ mol^{-1} for **TS(C3,C3′)**. The sign of the deviation does not appear to be systematic in this case. Also for the elimination pathways there are significant differences in energy of more than 10 kJ mol^{-1} for some of the stationary points between the MP2/6-31G(d) and the more accurate Gn_m data.

The complexation process and energetics are very similar for the H_2O–ROH_2^+ and NH_3–RNH_3^+ systems with the front side complexes (**X3**, **X** = **A**, **B**, **C**, and **D**) being the global energy minima in all cases. The stronger hydrogen bonds involving oxygen compared with nitrogen are reflected in the complexation energies, with the H_2O–ROH_2^+ species generally more strongly bonded than NH_3–RNH_3^+ by approximately 10–15 kJ mol^{-1}. The rear side minima (**X2**, **X** = **A**, **B**, and **D**) are approximately 50 kJ mol^{-1} higher in energy than the front side minima in Figs. 6, 7 and 9. The rear side minima are even more shallow than for H_2O–ROH_2^+ with the minimum **B2** below the transition structure **TS(B2,B3)** at the MP2/6-31G(d) level only as long as ZPVEs are not included. For the NH_3–$Pr^iNH_3^+$ system there is no MP2/6-31G(d) rear side minimum at all. As would be expected, the geometry of the transition structure for the transformation of the back side (**X2**, **X** = **A** and **B**) into the front side (**X3**) complex **TS(X2,X3)** is very similar to the **X2** geometry itself. For the NH_3–$Pr^iNH_3^+$ adduct we have calculated the transition state for the "space walk" of the NH_3 moiety from the structure **C3**, around $Pr^iNH_3^+$ and back to **C3** again. It is illustrated in Fig. 4 and denoted **TS(360° Rot.)**. There are minor geometry changes in the protonated amine moieties between the free protonated amines (**X1**, **X** = **A**, **B**, **C**, and **D**) and the complexes **X2** and **X3**.

Table 1 $G3_m$ dissociation energies for the reaction $RX^+ \longrightarrow R^+ + X$ (bond strengths) and vertical electron affinities and promotion energies G_r for RX^+ at the CCSD(T)/6-311++G(d,p)//MP2/6-31G(d) level. The promotion energies have been calculated applying ionization potentials for NH_3 and H_2O, 1026 and 1193 kJ mol^{-1}, respectively, calculated at the same level of theory. Total charges Q for the R and X moieties of RX^+ and the neutral RX· species have been calculated at the MP2/6-311++G(d,p)//MP2/6-31G(d) level employing the natural population analysis approach

RX	Bond strength, $D_{RX}{}^+$/kJ mol^{-1}	Vertical *EA*s/kJ mol^{-1}	G_r/kJ mol^{-1}	Q(R)–Q(X) for RX^+	Q(R) for RX·
$MeNH_3$	431	386	640	−0.32	0.24
$EtNH_3$	287	366	660	−0.29	0.26
Pr^iNH_3	233	352	674	−0.28	0.27
Bu^tNH_3	186	342	684	−0.25	0.27
$MeOH_2$	268	439	753	0.00	0.33
$EtOH_2$	139	410	783	0.06	0.38
Pr^iOH_2	97	389	804	0.11	0.40
Bu^tOH_2	59	369	824	0.15	0.42

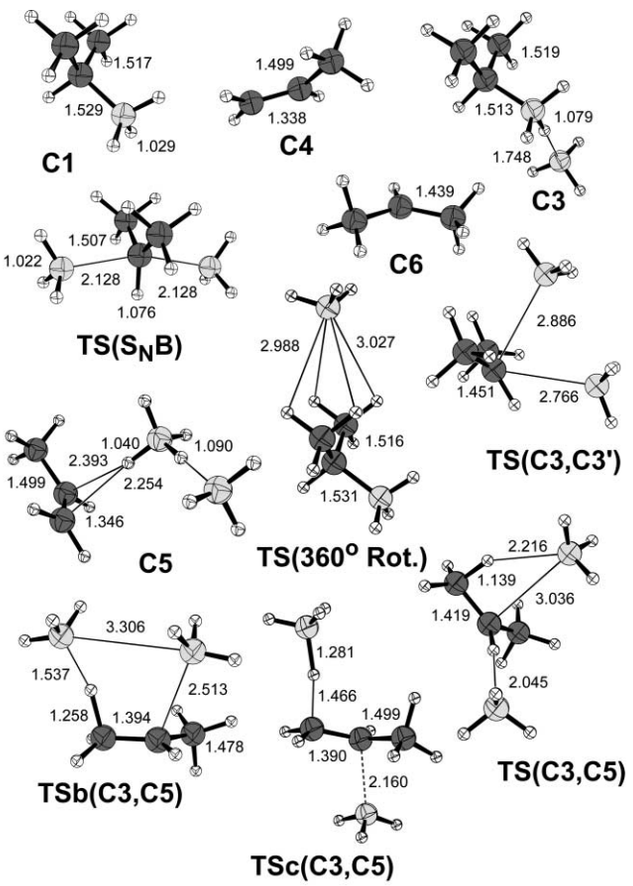

Fig. 4 Structures of stationary points on the PES for the substitution and elimination reaction between NH_3 and $Pr^iNH_3^+$ calculated at the MP2/6-31G(d) level. All bond lengths are given in Å. Cartesian coordinates for these structures have been included as Supplementary material. ‡ There is no rear-side energy minimum at the entrance channel for rear side substitution. The transition structure **TS(360° Rot.)** is for the space-walk of NH_3 around the $Pr^iNH_3^+$ moiety.

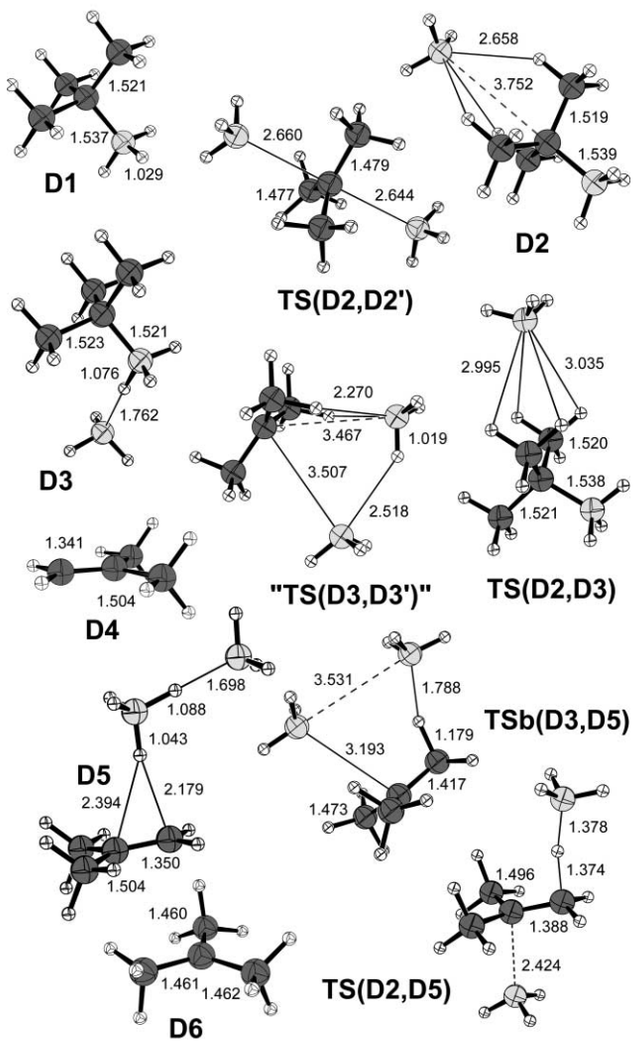

Fig. 5 Structures of stationary points on the PES for the substitution and elimination reaction between NH_3 and $Bu^tNH_3^+$ calculated at the MP2/6-31G(d) level. All bond lengths are given in Å. Cartesian coordinates for these structures have been included as Supplementary material. ‡ **"TS(D3,D3′)"** is a second order saddle point. See the text for further explanations.

The Walden inversion back side transition structures are given in Figs. 2–5 as **TS(X2,X2′)** (**X** = **A**, **B**, and **D**) and **TS(S$_N$B)** since there is no back side complex for the NH_3–$Pr^iNH_3^+$ system. The transition structures have a bond elongation compared with **X1** of the C_1–N bond being broken of 0.49 (R = Me), 0.53 (Et), 0.60 (Pr^i), and 1.11 Å (Bu^t), very similar to the situation in the H_2O–ROH_2^+ systems. The shortening of the N–C_1 bonds being formed between the rear side complexes **X2** (**X** = **A**, **B**, and **D**) and **TS(X2,X2′)** is fairly constant at 0.93, 1.06, and 1.09 Å, for R = Me, Et, and Bu^t, respectively, which is longer by approximately 0.3 Å than the H_2O–ROH_2^+ systems.

Ruggiero and Williams[6] and Uggerud and Bache-Andreassen[7] found that the Walden inversion nucleophilic substitution of the H_2O–$Bu^tOH_2^+$ adduct occurs in three sequential steps for which one of each of the three methyl groups rotates. For the Walden inversion of NH_3–$Bu^tNH_3^+$, there is only a single transition structure, **TS(D2,D2′)**, and the first and last of the three methyl rotations occur on the way up to and down from this transition state. This kind of reaction path is exactly what Ruggiero and Williams found for the reaction between Cl^- and Bu^tCl.[6] Notably, the ($G3_m$) Walden inversion reaction barrier increases steadily—$\Delta H^‡$ = 56 (R = Me), 73 (R = Et), 86 (R = Pr^i), and 101 kJ mol^{-1} ($R = Bu^t$)—with increasing alkyl substitution in agreement with earlier findings for the Cl^- + RCl reactions.[5,6] It thus appears that the inversion of this trend for H_2O–ROH_2^+ is particular for fairly weak nucleophiles, and that NH_3 already is strong enough for the return to the customary

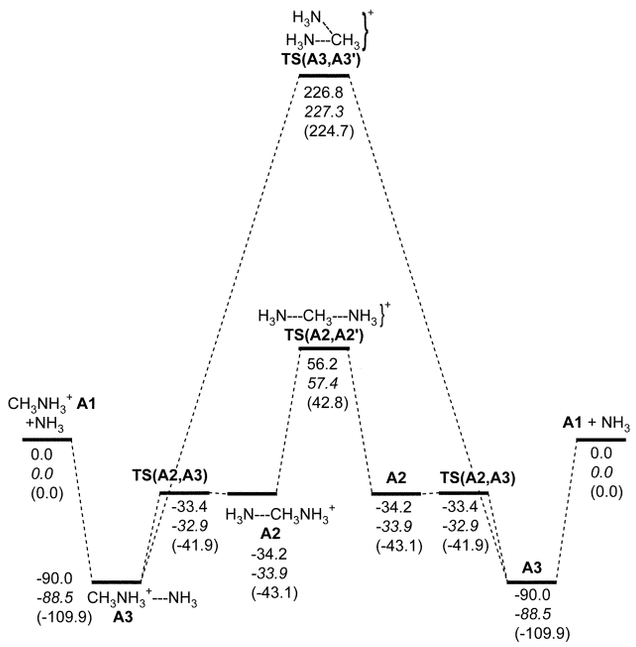

Fig. 6 Potential energy diagram for the substitution reaction between NH_3 and $MeNH_3^+$ calculated at the $G3_m$ level. The calculated energies at the $G2_m$ and MP2/6-31G(d) (including ZPVE corrections) level are given in italics and in parentheses, respectively. All relative energies are given in kJ mol^{-1} at 0 K.

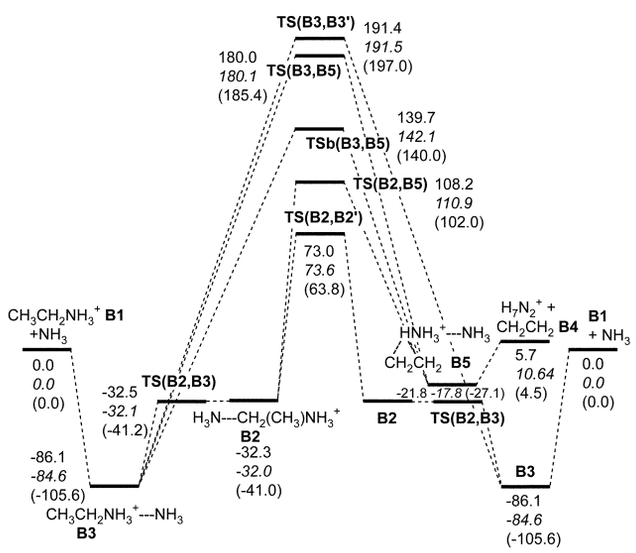

Fig. 7 Potential energy diagram for the substitution and elimination reaction between NH_3 and $EtNH_3^+$ calculated at the $G3_m$ level. The calculated energies at the $G2_m$ and MP2/6-31G(d) (including ZPVE corrections) level are given in italics and in parentheses, respectively. All relative energies are given in kJ mol^{-1} at 0 K.

relationship between alkyl substitution and barrier height. Note also that all energy barriers are so high that one would expect no reaction to occur under the conditions at which gas phase ion chemistry usually is performed. This is in full agreement with the experimental results (see the Introduction). The same is the case for both the S_NF and E2 pathways as seen from Figs. 6–9.

All front side substitution transition structures **TS(X3,X3′)** (**X** = **A**, **B**, and **C**) have much higher energy barriers than the corresponding rear side transition structures **TS(X2,X2′)**, and the C_1–N bond distances are also longer by between 0.2 and 0.7 Å. Despite significant efforts we were not able to locate a front side transition structure for the NH_3–$Bu^tNH_3^+$ system. None of our attempts led to transition structures

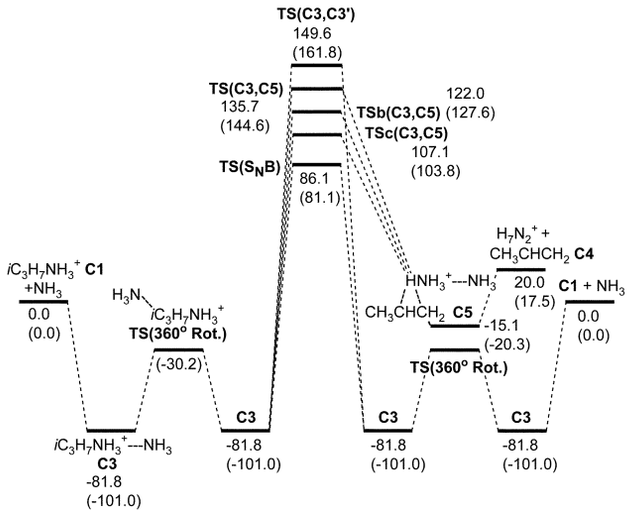

Fig. 8 Potential energy diagram for the substitution and elimination reaction between NH_3 and $Pr^iNH_3^+$ calculated at the $G3_m$ level. The calculated energies at the MP2/6-31G(d) level (including ZPVE corrections) are given in parentheses. All relative energies are given in kJ mol^{-1} at 0 K. There is no rear-side energy minimum at the entrance channel for rear side substitution. The transition structure **TS(360° Rot.)** is for the space-walk of NH_3 around the $Pr^iNH_3^+$ moiety.

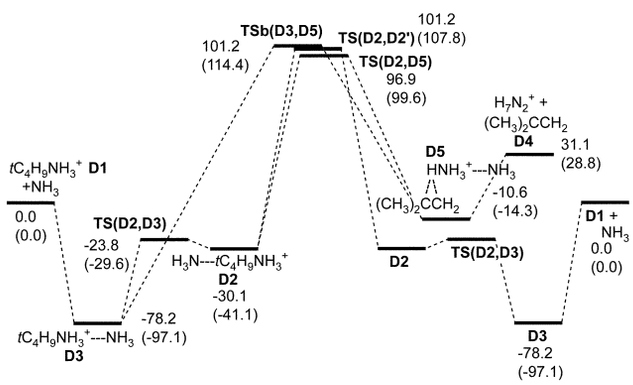

Fig. 9 Potential energy diagram for the substitution and elimination reaction between NH_3 and $Bu^tNH_3^+$ calculated at the $G3_m$ level. The calculated energies at the MP2/6-31G(d) level (including ZPVE corrections) are given in parentheses. All relative energies are given in kJ mol^{-1} at 0 K.

that correspond to a simple S_NF replacement, but instead to eliminations or simply to transition structures corresponding to conformational changes, mainly methyl group rotations. The second order saddle point "**TS(D3,D3′)**" of Fig. 5 with imaginary frequencies 86*i* and 103*i* cm^{-1} is our best candidate for a proper S_NF transition structure. The 86*i* cm^{-1} mode does appear to be a replacement of one for the other of the two NH_3 groups, while the higher 103*i* cm^{-1} mode corresponds to a rotation of the $(NH_3)_2$ "dimer" above the alkyl moiety. Attempts to follow this mode in order to obtain a proper S_NF transition structure were also unsuccessful. From the topology of the PES it is clear that any two minima (*e.g.* **D3** and **D3′**) may be connected with a path through only first order saddle points and minima. While we obviously cannot rule out the existence of a proper S_NF **TS(D3,D3′)** transition state, our failure to find such a geometry would indicate that the path connecting **D3** and **D3′** on the PES goes either through **TS(D2,D2′)** or *via* the "hidden pathway" for front side substitution. This pathway involves an elimination (*e.g.* **TSb(D3,D5)**), an exchange of the two ammonia molecules and a reversal over the **TSb(D3,D5)** transition structure. The second order saddle point **"TS(D3,D3′)"** is 21 kJ mol^{-1} above **TS(D2,D2′)** (MP2/6-31G(d) level) and indicates that S_NF-like trajectories should be possible approximately 20 kJ mol^{-1} above the **TS(D2,D2′)** S_NB pathway. Consequently,

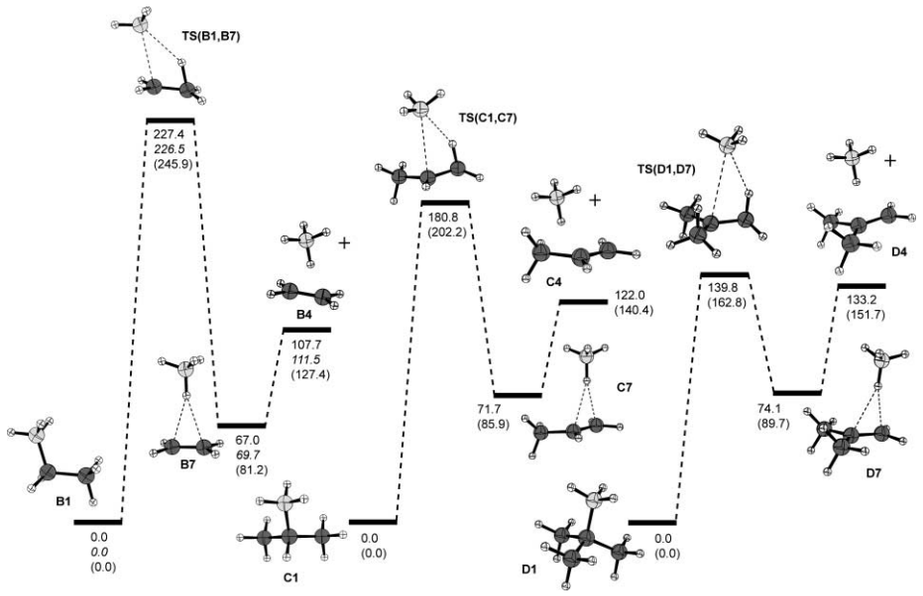

Fig. 10 Potential energy diagrams for the elimination of NH_4^+ from RNH_3^+ (R = Et, Pr^i, and Bu^t) calculated at the $G3_m$ level. The calculated energies at the $G2_m$ and MP2/6-31G(d) level (including ZPVE corrections) are given in italics and in parentheses, respectively. All relative energies are given in kJ mol^{-1} at 0 K.

as for the H_2O–ROH_2^+ systems, the difference in energy for rear and front side substitution sharply decreases along the series R = Me, Et, Pr^i, and Bu^t—from 171 kJ mol^{-1} (R = Me) to approximately 20 kJ mol^{-1} (R = Bu^t) for NH_3–RNH_3^+.

The elimination reaction PESs for

$$NH_3 + CH_3CR_1R_2–NH_3^+ \longrightarrow CH_2CR_1R_2 + N_2H_7^+, \quad (9)$$

(R_1,R_2 = H, CH_3) are given in Figs. 7–9. The intermediates **X5** (**X** = **B**, **C**, and **D**) are all below the energy of the reactants and the eliminations are only slightly exothermic. However, as for the substitution reactions, the reaction barriers are very high and no elimination was observed in the experiments. In the first article of this series,[8] we discussed the various pathways for elimination that are possible for the kind of systems that are studied here. Calculated $G3_m$ 0 K proton affinities for ammonia and the ammonia dimer are 850 and 946 kJ mol^{-1}, respectively. The experimental value is 854 kJ mol^{-1} for the ammonia molecule.[17,18] With the relevant alkene proton affinities in the range 670 to 800 kJ mol^{-1},[8] both the ammonia monomer and dimer should be able to eliminate the proton for the NH_3–RNH_3^+ systems, and this is also found in Figs. 7–9, with the transition structures illustrated in Figs. 3–5. For all three systems the lowest energy elimination (**TS(B2,B5)** for Et, **TSc(C3,C5)** for Pr^i, and **TS(D2,D5)**§ for Bu^t) is a proton elimination by an ammonia monomer, with the other ammonia molecule stabilizing the alkyl moiety from the rear side. Similarly for all three systems, the second lowest pathway (**TSb(B3,B5)** for Et, **TSb(C3,C5)** for Pr^i, and **TSb(D3,D5)** for Bu^t) is a proton abstraction by ammonia with the second ammonia molecule stabilizing the alkyl moiety at the front side. For the NH_3–$EtNH_3^+$ and NH_3–$Pr^iNH_3^+$ systems we found additional elimination pathways where the ammonia dimer abstracts the proton, but these were all slightly higher in energy than the transition structures **TS(B3,B5)** and **TS(C3,C5)**. These two pathways start at **X3**, the "spectator" ammonia molecule slides down to the C_1-hydrogen in the transition structures and then up again to create an ammonia dimer in **X5**. Despite significant effort we were unable to find any additional E2 transition structures for the NH_3–$Bu^tNH_3^+$ system.

§ There is actually a shallow rear side "exit channel" **D5′** minimum after the **TS(D2,D5)** transition structure, but the barrier to the front side minimum **D5** is only 7 kJ mol^{-1} at the MP2/6-31G(d) level.

Calculated PESs for the elimination of H_3O^+ from ROH_2^+ were given in the first article in this series.[8] The corresponding PESs for the elimination of NH_4^+ from RNH_3^+ are given in Fig. 10. Unlike the ROH_2^+ systems, all RNH_3^+ PESs have high elimination barriers.

Tentative analysis

The S_N2 reactivity for the NH_3–RNH_3^+ systems presented here and the reactivity for the H_2O–ROH_2^+ systems presented earlier[8] differ in at least two respects. Firstly, the NH_3–RNH_3^+ systems have much higher barriers than the H_2O–ROH_2^+ systems. This is also the case for the E2 reactions. Secondly, the NH_3–RNH_3^+ systems show the normal reaction barrier trend (NRBT) of higher barriers for the more alkyl substituted reaction centers. For the H_2O–ROH_2^+ systems, however, there is a non-NRBT trend with the more substituted systems having the lower Walden inversion reaction barriers.

In order to obtain some insight into these matters we have calculated several parameters that are summarized in Table 1. The R–X^+ bond strength against heterolytic cleavage (D_{RX^+}) is generally higher in RNH_3^+ than in ROH_2^+. This explains the differences between Fig. 10 of the current paper and Fig. 9 of our previous study,[8] *i.e.* the much higher barriers for elimination of XH^+ from H–R′X^+ for X = NH_3 than for H_2O. The bond strengths are important since the C_1–X bond has to be stretched significantly to reach the transition structure for elimination. The same arguments may be used to explain the much higher E2 barriers for the NH_3–RNH_3^+ compared with the H_2O–ROH_2^+ systems. Indeed, there is a nearly perfect correlation between elimination reaction barrier and D_{RX^+} for the reactions of Fig. 10 (correlation coeff. = 1.000) and for the **TSb(X3,X5)** type eliminations (correlation coeff. = 0.996).

The substitution reactions, on the other hand, involve simultaneous bond breaking and formation and earlier studies have been struggling to find a relationship between the bond strength of the bond being broken and reaction barriers. For example, Glukhovtsev *et al.*[26] have found that for the S_N2 reaction between Y^- and MeY (Y = F, Cl, Br, and I) there is a narrow range of reaction barriers (less than 20 kJ mol^{-1}) compared with a large variation in Me–Y bond strengths (230 kJ mol^{-1}). The order of bond strengths (F > Cl > Br > I) is also different from the order of reaction barriers (Cl > F ≥ Br > I). The most recent and accurate results for these reactions have recently been reviewed.[10] On the other hand, the S_N1 process,

$$X + R–X^+ \longrightarrow X + R^+ + X \longrightarrow X–R^+ + X \qquad (10)$$

with a complete removal of the leaving group before the formation of the bond to the entering nucleophile, provides an upper limit for the reaction barrier for the gas phase S_N2 reaction. Consequently, a system with a weak bond being broken (*e.g.* $Bu^tOH_2^+$ with $D_{RX^+} = 59$ kJ mol^{-1}) must necessarily have a lower nucleophilic substitution barrier than the high barrier NH_3–RNH_3^+ systems with $\Delta H^{\ddagger}$ in the range 56 to 101 kJ mol^{-1}.

The valence bond state correlation diagram (VBSCD) approach of Shaik, Pross, and co-workers[12,27,28] is currently among the few theories that are available for illuminating the S_N2 reactivity differences summarized above. It describes the formation of the barrier for the central S_N2 reaction step as due to the avoided crossing of two curves comprising the reactant- and product-like Heitler–London (HL) valence bond (VB) states with additional VB states mixed in. The ground state HL structure **1** and the additional attractive VB structure **2** are illustrated in Scheme 1. The S_N2 barrier arises at the lower energy profile that is created due to the avoided crossing of the two VB state curves and the barrier height is given by the model,

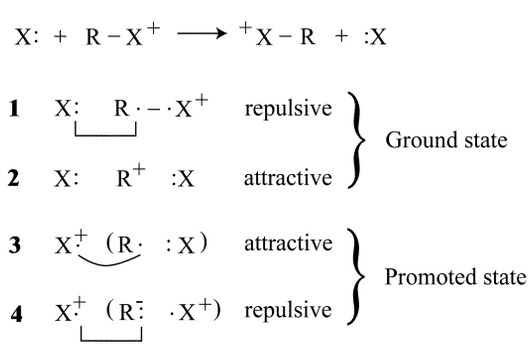

Scheme 1 Valence bond structures involved in the ground and promoted state for the cationic identity S_N2 reaction.

$$\Delta E^{\neq}_{CB} = fG_r - B \qquad (11)$$

where B is the avoided crossing interaction ("resonance interaction energy"), G_r is the promotion gap and f a curvature factor. The two most significant promoted state VB structures for the cationic S_N2 reactions are **3** and **4** in Scheme 1. The parameter B cannot easily be calculated employing molecular orbital theory and does not correspond to any physical observable. While it has been approximated from VB calculations and HOMO–LUMO gaps at the transition state, we follow the approach of some earlier studies, neglect variations in this parameter and assume it is semi-constant for the current reactions.

For these systems the promotion energy may be approximated by

$$G_r = IP_X - EA_{RX^+} \qquad (12)$$

where IP_X is the vertical ionization energy of X (NH_3 or H_2O) and EA_{RX^+} is the vertical electron affinity of RX^+ (protonated amine or alcohol). The calculated promotion energies G_r are given in Table 1 together with the other parameters of eqn. (12). According to VBSCD the promotion energy is the origin of the reaction barrier, but it is the interplay of f and G_r that determines the barrier. Considering the above approximations, the results of Table 1 clearly show that the f factor must be quite different for the NH_3–RNH_3^+ and H_2O–ROH_2^+ systems. The promotion energies are the highest for H_2O–ROH_2^+, but still all the reaction barriers are much lower than for any of the NH_3–RNH_3^+ systems.

The charge difference Q(R)–Q(X) of Table 1 is always strongly negative for RNH_3^+ while it is positive for ROH_2^+. This indicates that a larger fraction of VB structure **2** is involved in the ground state for ROH_2^+ than for RNH_3^+. According to the rules of the VBSCD scheme (Rule 5 of Shaik and Shurki[27]), a large fraction of the attractive VB structure **2** in the ground state at the expense of the HL VB structure **1** leads to a smaller f value and lower reaction barrier. This is in accordance with our findings. VBSCD Rule 4 of Shaik and Shurki[27] may also be used to explain our results. The two VB structures **3** and **4** both contribute to the promoted state, but a higher contribution of **4** gives a more delocalized promoted state, a higher f and a higher reaction barrier. Hence, the more negative is the charge on R in the promoted state, the higher is the barrier. Indeed it is found that Q(R) for RX· is smaller for RNH_3 than for ROH_2 (Table 1). The lower Walden inversion barriers for X = H_2O compared with NH_3 are consequently connected both with the larger group electronegativity of H_2O and with the weaker D_{RX^+} bond strengths for ROH_2^+ compared with RNH_3^+. Similar findings have previously been reported by Lee *et al.*[29] for allyl transfer reactions. For a system with a higher electronegativity of X the structural and electronic reorganization required to reach the transition state is reduced and the activation barrier is lowered.

A similar analysis might shed some light on the non-NRBT for the H_2O–ROH_2^+ system. G_r increases steadily with increasing alkyl substitution and non-bonding interactions not accounted for within this model should also give the same trend. While the results are not clear-cut the charge parameters described above are consistent with a sharper decrease of f from Me to Bu^t for H_2O–ROH_2^+ than for NH_3–RNH_3^+ and accompanying reduced barriers. For H_2O–ROH_2^+ Q(R)–Q(X) for RX^+ and Q(R) for RX· increase smoothly by +0.15 and +0.09 from Me to Bu^t. For NH_3–RNH_3^+ the values tend to be slightly more stable, increasing by +0.07 and +0.03, respectively. At the same time, the limiting barrier of reaction (10) is more important for the H_2O–ROH_2^+ system due to the weaker RX^+ bonds.

Conclusion

High level *ab initio* theory has in the current work been employed in a study of reaction barriers for systems for which no experimental low energy reaction rate data are or are likely to become available. The results for the NH_3–RNH_3^+ system have been analyzed and compared with previous results for the related H_2O–ROH_2^+ system. Several parameters have been found to correlate with the S_N2 reaction barriers—the charge difference Q(R)–Q(X) for RX^+ which is strongly coupled with the group electronegativity of X, the RX^+ bond strength, and additional non-bonding effects. In addition parameters such as the promotion energy of eqn. (12) are of some significance. From the currently rather low number of similar reactions studied, it is therefore difficult to generate any quantitative rules for determining S_N2 reaction barriers, and studies of more related systems seem to be in place. We are currently undertaking such a study of the HF–RFH^+ system.[20] Unsurprisingly, for the NH_3–RNH_3^+ E2 reaction, a strong correlation between the R–NH_3^+ bond strength and reaction barrier was found.

While the S_NB transition structures were rather easy to locate, the large number of competing E2 and S_NF pathways for the larger species made it very time consuming to investigate these reactions properly. It is also unlikely that statistical methods such as for example Rice–Ramsberger–Kassel–Marcus (RRKM) theory will be successful in determining accurate reaction rates and in particular branching rates on the very complicated PESs that may contain significantly more than five competing E2 and S_N2 pathways within a rather narrow energy range. Obviously, reacting systems are dynamical and do not necessarily follow IRC pathways and the large amount of manual work involved in locating minima and in

particular transition structures makes it tempting to consider alternatives for species of the complexity that is considered here—in particular direct molecular mechanics analyzed methods.

Acknowledgements

The authors wish to thank NFR (The Norwegian Research Council) for financial support through a postdoctoral fellowship for JKL. We are also grateful for a generous grant of computing time from NOTUR (The Norwegian High Performance Computing Consortium).

References

1 C. K. Ingold, *Structure and Mechanism in Organic Chemistry*, Cornell University Press, Ithaca, NY, 1953.
2 M. B. Smith and J. March, *March's Advanced Organic Chemistry: Reactions, Mechanisms, and Structure*, 5th edn., Wiley, New York, 2001.
3 A. Streitwieser, Jr., *Solvolytic Displacement Reactions*, McGraw-Hill, New York, 1962.
4 D. F. DeTar, D. F. McMullen and N. P. Luthra, *J. Am. Chem. Soc.*, 1978, **100**, 2484.
5 F. Jensen, *Chem. Phys. Lett.*, 1992, **196**, 368.
6 G. D. Ruggiero and I. H. Williams, *J. Chem. Soc., Perkin Trans. 2*, 2001, 448.
7 E. Uggerud and L. Bache-Andreassen, *Chem. Eur. J.*, 1999, **5**, 1917.
8 J. K. Laerdahl and E. Uggerud, *Org. Biomol. Chem.*, 2003, DOI: 10.1039/b302268d (preceding paper).
9 W. N. Olmstead and J. I. Brauman, *J. Am. Chem. Soc.*, 1977, **99**, 4219.
10 J. K. Laerdahl and E. Uggerud, *Int. J. Mass Spectrom.*, 2002, **214**, 277.
11 S. Gronert, *Chem. Rev.*, 2001, **101**, 329.
12 S. S. Shaik, H. B. Schlegel and S. Wolfe, *Theoretical Aspects of Physical Organic Chemistry: The S_N2 Reaction*, John Wiley, New York, 1992.
13 R. A. Marcus, *Annu. Rev. Phys. Chem.*, 1964, **15**, 155.
14 M. J. Pellerite and J. I. Brauman, *J. Am. Chem. Soc.*, 1980, **102**, 5993.
15 M. J. Pellerite and J. I. Brauman, *J. Am. Chem. Soc.*, 1983, **105**, 2672.
16 M. L. Chabinyc, S. L. Craig, C. K. Regan and J. I. Brauman, *Science*, 1998, **279**, 1882.
17 E. P. Hunter and S. G. Lias, *J. Phys. Chem. Ref. Data*, 1998, **27**, 413.
18 P. J. Linstrom and W. G. Mallard (Eds.), *NIST Chemistry WebBook, NIST Standard Reference Database Number 69*, National Institute of Standards and Technology, Gaithersburg, MD 20899 (http://webbook.nist.gov), 2001.
19 J. D. D. Martin and J. W. Hepburn, *J. Chem. Phys.*, 1998, **109**, 8139.
20 P. U. Civcir, L. Bache-Andreassen, J. K. Laerdahl, K. Faegri, Jr. and E. Uggerud, manuscript in preparation.
21 M. J. Frisch, G. W. Trucks, H. B. Schlegel, G. E. Scuseria, M. A. Robb, J. R. Cheeseman, V. G. Zakrzewski, J. A. Montgomery, Jr., R. E. Stratmann, J. C. Burant, S. Dapprich, J. M. Millam, A. D. Daniels, K. N. Kudin, M. C. Strain, O. Farkas, J. Tomasi, V. Barone, M. Cossi, R. Cammi, B. Mennucci, C. Pomelli, C. Adamo, S. Clifford, J. Ochterski, G. A. Petersson, P. Y. Ayala, Q. Cui, K. Morokuma, P. Salvador, J. J. Dannenberg, D. K. Malick, A. D. Rabuck, K. Raghavachari, J. B. Foresman, J. Cioslowski, J. V. Ortiz, A. G. Baboul, B. B. Stefanov, G. Liu, A. Liashenko, P. Piskorz, I. Komaromi, R. Gomperts, R. L. Martin, D. J. Fox, T. Keith, M. A. Al-Laham, C. Y. Peng, A. Nanayakkara, M. Challacombe, P. M. W. Gill, B. G. Johnson, W. Chen, M. W. Wong, J. L. Andres, C. Gonzales, M. Head-Gordon, E. S. Replogle and J. A. Pople. Gaussian 98 (Revision A.11); Gaussian, Inc.: Pittsburgh, PA, 2001.
22 L. A. Curtiss, K. Raghavachari, G. W. Trucks and J. A. Pople, *J. Chem. Phys.*, 1991, **94**, 7221.
23 L. A. Curtiss, K. Raghavachari, P. C. Redfern, V. Rassolov and J. A. Pople, *J. Chem. Phys.*, 1998, **109**, 7764.
24 A. P. Scott and L. Radom, *J. Phys. Chem.*, 1996, **100**, 16502.
25 A. E. Reed, R. B. Weinstock and F. Weinhold, *J. Chem. Phys.*, 1985, **83**, 735.
26 M. N. Glukhovtsev, A. Pross and L. Radom, *J. Am. Chem. Soc.*, 1995, **117**, 2024.
27 S. Shaik and A. Shurki, *Angew. Chem., Int. Ed.*, 1999, **38**, 586.
28 S. Shaik, *Valence bond curve crossing models*, in *Encyclopedia of computational chemistry*, P. v. R. Schleyer (Ed.), John Wiley, Chichester, UK, 1998, Vol. 5, p. 3143.
29 I. Lee, C. K. Kim and B.-S. Lee, *J. Phys. Org. Chem.*, 1995, **8**, 473.